Research Square

Preprints are preliminary reports that have not undergone peer review.
They should not be considered conclusive, used to inform clinical practice,
or referenced by the media as validated information.

Imaging-derived wall shear stress and strain reflect local mechanical vulnerability in BAV aortic aneurysm

Louise Neave
University of Calgary
Miriam Nightingale
University of Calgary
Richard Beddoes
ViTAA Medical Solutions
Anshul S. Jadli
University of Calgary
Vaibhav B. Patel
University of Calgary
Julio Garcia
University of Calgary
Paul W.M. Fedak
University of Calgary
Elena S. Di Martino
edimarti@ulcalgary.ca

University of Calgary

Research Article

Keywords: aortic aneurysm, biomechanics, wall strain, MR 4D flow, bicuspid aortic valve

Posted Date: November 23rd, 2026

DOI: https://doi.org/10.21203/rs.3.rs-11380582/v1

License: This work is licensed under a Creative Commons Attribution 4.0 International License.
Read Full License

Additional Declarations: Competing interest reported. E.D.M. is a co-founder, Chief Scientific Officer, and minority shareholder of ViTAA Medical Solutions. R.B. is the Chief Technology Officer of ViTAA Medical

Solutions. L.N. is an employee of ViTAA Medical Solutions. The remaining authors declare that they have no known competing financial interests or personal relationships that could have appeared to influence the work reported in this paper.

Imaging-derived wall shear stress and strain reflect local mechanical vulnerability in BAV aortic aneurysm

Louise Neave[1,2,3], Miriam Nightingale[1,2], Richard Beddoes[4], Anshul S. Jadli[2,5], Vaibhav B. Patel[2,5], Julio Garcia[2,6,7], Paul W.M. Fedak[2,7], Elena S. Di Martino[1,2,3]

[1] Department of Biomedical Engineering, University of Calgary, Calgary, AB, Canada

[2] Libin Cardiovascular Institute, University of Calgary, Calgary, AB, Canada

[3] R&D Department, ViTAA Medical Solutions, Montreal, QC, Canada

[4] Product Development Department, ViTAA Medical Solutions, Montreal, QC, Canada

[5] Department of Physiology and Pharmacology, University of Calgary, Calgary, AB, Canada

[6] Department of Radiology, University of Calgary, Calgary, AB, Canada

[7] Department of Cardiac Sciences, University of Calgary, Calgary, AB, Canada

Corresponding Author:

Elena S. Di Martino

Department of Biomedical Engineering

University of Calgary

Calgary, AB, Canada

Email: edimarti@ulcalgary.ca

Acknowledgments

Funding for this project was provided by the National Institutes of Health grant (NIH HL133504 PWMF, ESDM) and Natural Sciences and Engineering Research Council of Canada Discovery Grants Program (RGPIN-07178 ESDM, RGPIN-2020-04549 and DGECR-2020-00204 JG), and NSERC Alliance – Alberta Innovates Advance Program (#232403115 JG).

ABSTRACT

BAV-associated ascending aortic aneurysm is primarily assessed by maximum diameter, which provides limited insight into regional wall integrity and mechanical properties. This study investigated non-invasive, imaging-derived wall shear stress (WSS) and local wall strain reflect region- and layer-specific aortic properties through a multi-scale analysis integrating in vivo biomechanics, RNA expression, and ex vivo mechanical testing. Ascending aortic aneurysm specimens were collected from 10 BAV patients and tissue samples were spatially matched to local imaging measurements. Biaxial, uniaxial, and delamination testing was conducted to characterize the mechanical behaviour of the composite wall, media, adventitia, and layer interface, while quantitative real-time PCR was used to assess *COL1A1* and *COL3A1* expression. Higher WSS was associated with evidence of localized tissue remodeling, including reduced medial transition-zone onset, reduced medial thickness, and greater energy loss in the media, adventitia, and composite wall. WSS was also positively associated with collagen gene expression, suggestive of increased matrix remodeling activity. Higher wall strain was associated with reduced axial strength and stiffness in the composite wall and adventitia, together with reduced medial stiffness. Increasing age was associated with widespread decrease in the mechanical properties of the wall layers and interface, while maximum diameter showed fewer associations with the tissue properties evaluated. These findings demonstrate distinct associations between imaging-derived WSS and wall strain and local aortic wall properties, with WSS relating predominantly to medial remodeling and strain to reduced tissue stiffness and strength. Together, these findings support further investigation of WSS and wall strain as non-invasive markers associated with regional aortic wall mechanical properties in BAV-associated ascending aortic aneurysm.

Keywords: aortic aneurysm, biomechanics, wall strain, MR 4D flow, bicuspid aortic valve

Statements and Declarations

E.D.M. is a co-founder, Chief Scientific Officer, and minority shareholder of ViTAA Medical Solutions. R.B. is the Chief Technology Officer of ViTAA Medical Solutions. L.N. is an employee of ViTAA Medical Solutions. The remaining authors declare that they have no known competing financial interests or personal relationships that could have appeared to influence the work reported in this paper.

1 INTRODUCTION

Ascending aortic aneurysm (AsAA) is a clinically significant and often asymptomatic condition characterized by progressive dilation of the aorta and an increased risk of adverse events, including aortic dissection and rupture. Clinical management is currently guided primarily by maximum aortic diameter, with surgical intervention recommended once population-based thresholds are reached. However, studies have shown that complications can occur at sizes below the current 5.5 cm surgical threshold (Pape et al. 2007; Saliba et al. 2015; Perez et al. 2023; Wu et al. 2023), demonstrating that diameter alone does not capture patient-specific variation in wall integrity, regional tissue remodeling, or mechanical stability. Although there is growing consensus that diameter is an inadequate criterion for guiding treatment strategies in AsAA, alternative measures have not yet been widely accepted or adopted in clinical practice.

This challenge is particularly relevant in patients with bicuspid aortic valve (BAV), a congenital condition occurring in approximately 1% of the population (Fedak et al. 2002). BAV is characterized by the formation of an abnormal aortic valve with two cusps and is associated with an increased incidence and accelerated progression of cardiovascular complications affecting both the valve and the ascending aorta (Ward 2000). In BAV-associated AsAA, valve-mediated abnormalities in aortic hemodynamics have been linked to regional wall remodeling, including extracellular matrix degradation, elastin fragmentation, and altered tissue structure (Yang et al. 2025). These microstructural changes are associated with adverse changes in tissue mechanics, including altered stiffness and reduced elastic recoil (Iliopoulos et al. 2009; Chung et al. 2014; Nightingale et al. 2022a).

The mechanical integrity of the aortic wall is determined by the structural and mechanical roles of its three distinct layers: the intima, media, and adventitia. The media, composed of organized elastin, smooth muscle cells, and collagen fibres, is particularly important for maintaining the elastic recoil and load-bearing behaviour of the aorta, while the adventitia provides additional structural support at higher levels of deformation. In AsAA, disease-driven remodeling affects the wall non-uniformly through its thickness, resulting in layer-specific changes in mechanical behaviour (Sokolis et al. 2012; Deveja et al. 2018). This heterogeneity is clinically relevant as both aortic dissection and rupture are the result of local tissue failure. Aortic dissection initiates with an intimal tear followed by propagation of blood between the wall layers, whereas rupture involves full-thickness failure of the aortic wall. Because dissection is driven by failure within the medial layer, layer-specific mechanical assessment can provide insight into mechanisms of wall failure that may not be captured by composite tissue testing alone.

Ex vivo biomechanical testing remains the gold standard for characterizing the mechanical consequences of aneurysm remodeling and is essential for understanding how changes in tissue structure may contribute to these clinically relevant failure modes. Previous studies have demonstrated substantial inter- and intra-patient variability in aortic tissue properties, suggesting that wall condition is both patient-specific and spatially heterogenous (Choudhury et al. 2009; Guzzardi et al. 2017; Bollache et al. 2018; Angouras et al. 2019a). This regional variability highlights the potential value of non-invasive identification of localized wall weakening, rather than relying on global measures that assume uniform degeneration throughout the aneurysm. Advances in imaging technology increasingly support this approach by enabling clinically relevant features of the aortic environment to be assessed non-invasively and with spatial resolution. Parameters such as wall shear stress and wall deformation can provide insight into the local hemodynamic and mechanical conditions experienced by the aortic wall (Bollache et al. 2018;

Forneris et al. 2020; Yang et al. 2025). Because these in vivo measures may reflect the underlying tissue remodeling and mechanical integrity, they represent a promising alternative to risk assessment versus diameter alone.

This study aimed to evaluate the relationships between in vivo parameters and spatially matched ex vivo mechanical properties of BAV-AsAA tissue, tested as both layer-separated and composite to fully capture the heterogenous remodelling characteristics. Establishing these relationships may provide a foundation for future development of imaging-based biomarkers capable of identifying regional wall vulnerability and improving patient-specific risk prediction.

2 METHODS

2.1 Patient population and tissue samples

Specimens were obtained from BAV AsAA patients undergoing elective ascending aortic resection between 2019 and 2021 at the Foothills Medical Centre (Calgary, AB, Canada) under the approval of the Conjoint Faculties Research Ethics Board (REB14-0084). Resected whole aortic aneurysm rings were divided first by anatomical region (greater curvature, lesser curvature, posterior, and anterior), and then further divided into specimens for mechanical testing and gene expression analysis based on the region size (Fig. 1). It is assumed that the division of specimens releases residual stresses in the tissue, so that all pieces are in a zero-stress configuration prior to further testing and analysis. Specimens were marked to preserve the axial and circumferential orientation. From each specimen, one circumferential and one axial strip were prepared for uniaxial and delamination testing, while the remaining square section was used for biaxial tensile testing.

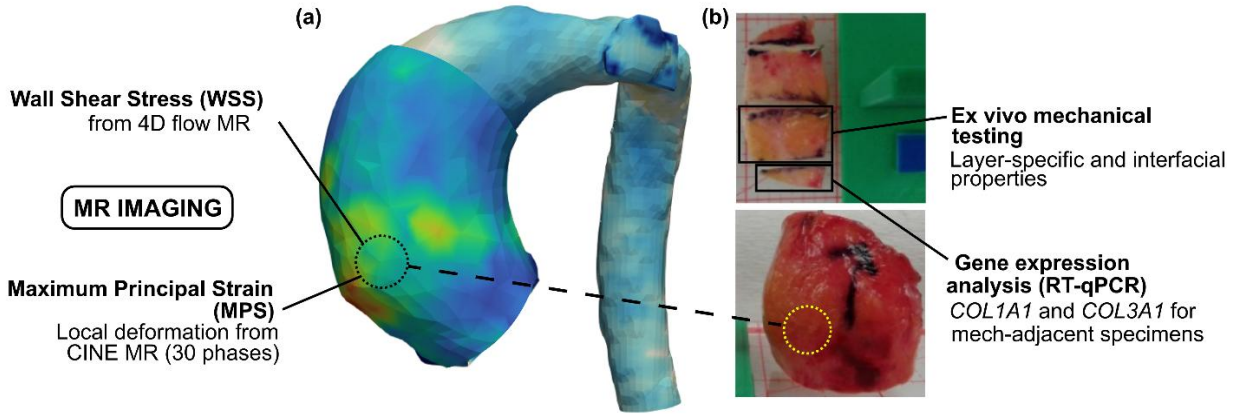

Fig. 1 Methods overview. (a) *In vivo* MR imaging was used to quantify local wall shear stress and maximum principal strain; (b) The corresponding virtual sample location was spatially matched to the excised aneurysm ring, which was subdivided into anatomical regions and individual specimens for mechanical testing and gene expression analysis.

2.2 Mechanical testing

A combination of delamination testing, biaxial tensile testing, and uniaxial tensile testing was used to characterize the mechanical behaviour of the tissue samples. For delamination testing, a separation was initiated manually at the natural delamination plane (Angouras et al. 2019b) in each circumferential or axial strip. The separation was carefully extended to about ¼ of the sample

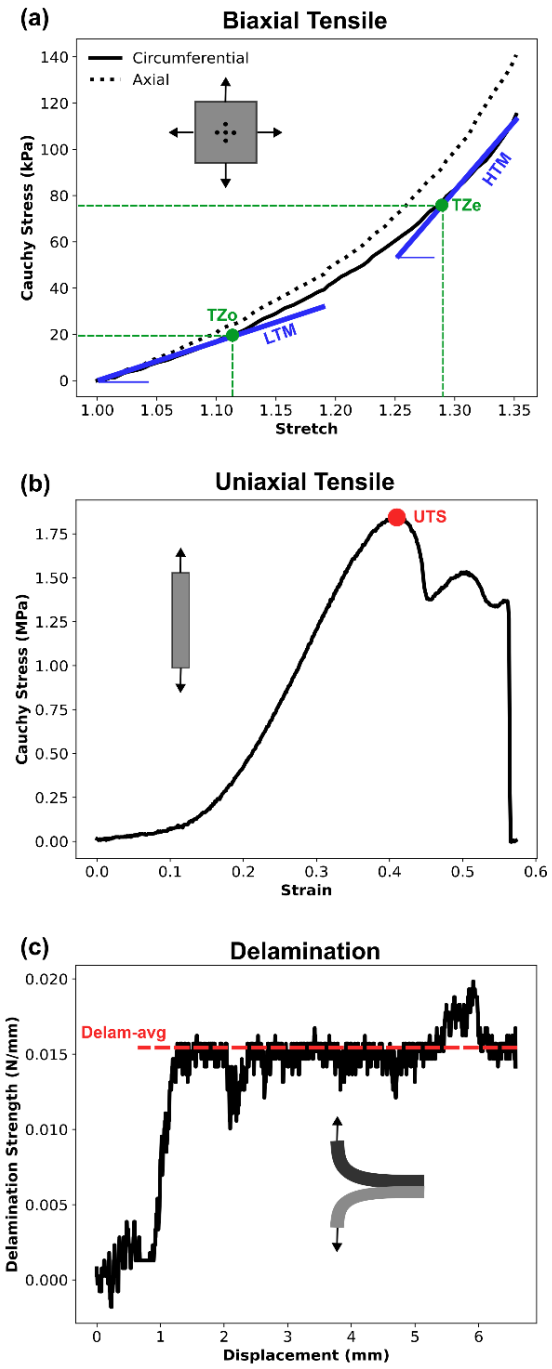

Fig. 2 Ex vivo mechanical analysis. (a) Biaxial tensile testing was used to determine the low-strain tangential modulus (LTM), high-strain tangential modulus (HTM), transition-zone onset (TZo) stress and stretch, transition-zone end (TZe) stress and stretch, and energy loss. (b) Uniaxial tensile testing was used to determine ultimate tensile strength (UTS). (c) Delamination testing was used to determine delamination strength (Delam-avg) as a measure of interfacial strength. All variables were evaluated in the axial and circumferential directions.

length, and the layers were clamped in opposing grips in a vertical uniaxial testing system (CellScale Biomaterials Testing, Waterloo, ON). The specimens were submerged in PBS solution at 37°C and a vertical displacement was applied at 1 mm/min until complete delamination of the specimen was achieved. Delamination tension was calculated as the recorded tensile force normalized by the unloaded specimen width, and delamination strength was determined as the average delamination tension after the initial peak (Angouras et al. 2019b).

For both uniaxial and biaxial tensile testing, both composite and layer-specific data was collected from neighbouring specimens. In the layer-specific samples, the tissue was separated into two layers: a media-dominated layer consisting of intima-media tissue up to the natural delamination plane, and adventitia-dominated layer consisting of tissue from the delamination plane to the external adventitial surface. Uniaxial tensile testing was performed on a uniaxial mechanical testing system equipped with a 10N load cell (CellScale Biomaterials Testing, Waterloo, ON) using the layer-separated strips generated from delamination testing after removal of the clamped ends, or strips cut from adjacent composite specimens. Each sample was subjected to a preconditioning protocol of 10 cycles to 15% strain at 1 Hz, followed by a failure protocol in which a 10 mm/min displacement was applied to the specimen until failure occurred. Recorded force and displacement values were converted to Cauchy stress and engineering strain, and the ultimate tensile strength (UTS) was defined as the first significant local maxima.

Biaxial tensile testing was performed on composite and layer-separated specimens using a four-motor biaxial testing system equipped with two 22N load cells (ElectroForce Systems, TA Instruments, Springfield, MO). Specimens were cut to squares of edge length 10 mm and thickness measurements recorded at 2 locations. Five markers were applied to the central region of the specimen using graphite and cyanoacrylate glue for optical strain tracking. The samples were then mounted to the machine using hooks and submerged in PBS solution at 37°C. A preload of 0.05 N was applied to remove slack, and a series of displacement-controlled protocols applied to

a maximum of 60% global strain, followed by maximum 80% global strain where possible. Each protocol consisted of five displacement-controlled cycles at 0.1 Hz, with varied circumferential-axial ratios of strain. Biaxial stress-stretch data were analyzed from the last cycle to extract mechanical properties of the sample. As previously described (Nightingale et al. 2022a), the parameters used to characterize the nonlinear behaviour of the tissue included the low-strain tangential modulus (LTM), high-strain tangential modulus (HTM), the transition zone onset and end stresses (TZo and TZe), and the global energy loss (EL) (Fig. 2).

2.3 RT-qPCR analysis

Total RNA was extracted from adjacent specimens using the TRIzol reagent (#15–596–018, Thermo Fisher Scientific) according to the manufacturer's instructions. Extracted RNA was dissolved in RNase-free water, and total RNA concentration was determined using SpectraMax iD3 (Molecular Devices, CA, United States). As described previously(Ballasy et al. 2021), RT-qPCR was performed by first preparing the cDNA Reverse Transcription Kit (#4374966, Thermo Fisher Scientific), and gene expression was measured using TaqMan probes for *COL1A1* (Hs.PT.58.15517795), *COL3A1* (Hs.PT.58.4249241), and *18s RNA* (Hs.PT.39a.22214856.g). For each gene, a standard curve was generated using known concentrations (0.1, 1, 10, 100, 1000 ng) of cDNA as a function of cycle threshold. Analysis of the gene expression was performed with TaqMan Real-time PCR using QuantStudio system (Thermo Fisher Scientific, MA, United States), and data analysis was completed using QuantStudio design and analysis software (version 1.4.3). Samples were run in triplicate and 18S rRNA was used as an endogenous control.

2.4 In vivo analysis

Cine MR image stacks for in vivo strain calculations were collected using a 3-Tesla Siemens Prisma model scanner at the Stephenson Cardiac MRI Center (Foothills Medical Center, Calgary, Alberta). Image acquisition had a 70% k-space coverage, a 256 x 200 in plane matrix, and a slice thickness of 6 mm with a 0.6 mm gap (10%). Cardiac-gated series with 30 frames were collected, with approximately 25 slices in the thoracic region. The X-Y plane resolution of voxels was 1.4 mm. 4D flow MR images were collected during the same session using the same machine and the 4D flow images were used to generate a WSS point cloud (Van Ooij et al. 2015). The MR image stacks were then segmented to mask the aortic wall using commercial third-party software SimpleWare (Synopsys, Mountain View, CA). Resulting masks were smoothed using a Gaussian smoothing filter, and a triangular surface mesh was generated and reduced to the lowest supported mesh resolution (maximum coarseness).

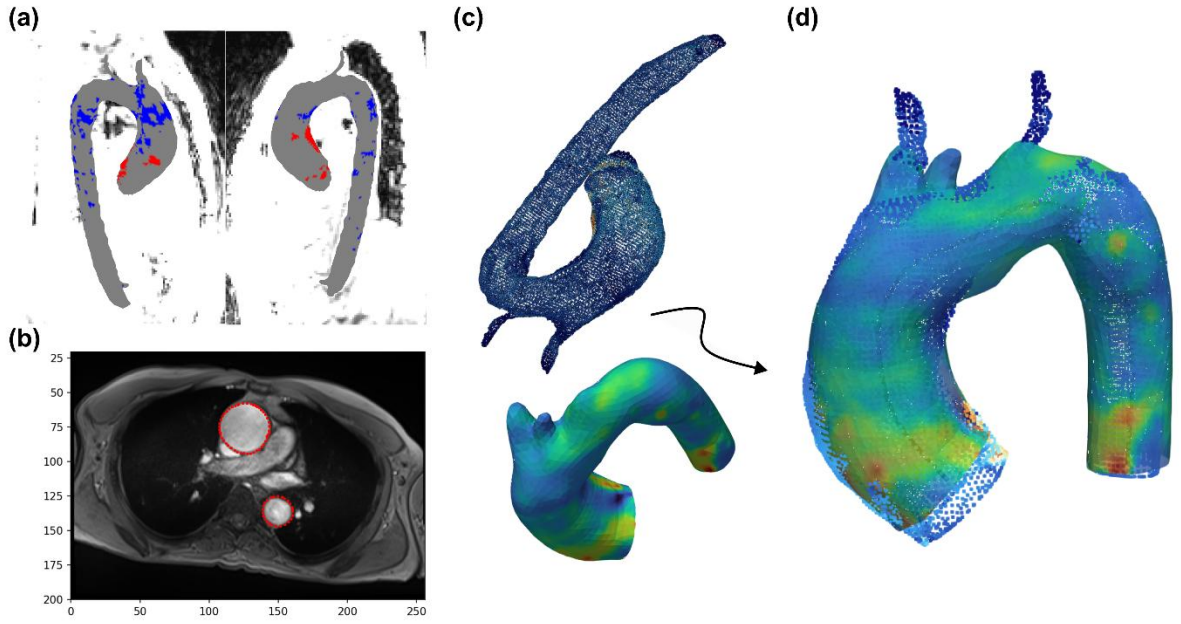

Fig. 3 In vivo imaging and registration. (a) WSS data is derived from 4D flow MR imaging; (b) An optical-flow algorithm is applied to CINE-MR image stacks for tracking of 2D aortic wall contours across 30 cardiac phases; (c) WSS point cloud data (top) is transformed outside of the strain mesh (bottom) image space and must be registered prior to specimen selection; (d) Registration of the WSS and strain meshes is applied based on centerline and surface alignment optimization.

2.3.1 Strain analysis

In vivo aortic wall strain was calculated from the cine MR image series using a custom optical flow pipeline in Python (version 3.9.22, Python Software Foundation). The extracted surface meshes for each subject were registered back to the image stack, and the mesh intersected with each image slice to generate a closed contour representation of the aortic wall at each through-plane location. Image spacing and DICOM spatial metadata were used to preserve physical coordinates. Because of the limited through-plane resolution, displacements were tracked using a 2D optical flow algorithm (van der Walt et al. 2014). X-Y displacements were estimated slice by slice, while the original Z position of the nodes was preserved. The resulting tracked contours were smoothed using local spatial interpolation to reduce circumferential jitter. For each phase, the cross-sectional area was calculated from the 2D contours in each slice and summed across all slices to estimate the total luminal area. The diastolic phase was then defined as the phase with the minimum summed contour area, and the systolic phase was defined as the phase with maximum summed area.

The tracked contour positions were then reconstructed into phase-specific 3D surface meshes. For each mesh node, neighbouring tracked contour points were identified using a nearest-neighbour search and the local displacement was calculated using inverse-distance weighting. The smoothed nodal position was then found as the reference position plus the weighted average displacement of the neighbouring tracked points. This method preserves the phase-specific motion estimated from the 2D contour tracking while producing 3D surfaces that are suitable for local deformation analysis.

Using the smoothed 3D surface geometries, the displacement was calculated between the diastolic and systolic meshes. The displacement vector at each node was defined as the difference between the systolic and diastolic coordinates, and then the strain was computed from the local change in mesh geometry between the two phases. For each triangular surface element, the deformation gradient was calculated from the change in local edge vectors of the triangle. The right Cauchy-Green deformation tensor ($\mathbf{C} = \mathbf{F}^{\mathbf{T}}\mathbf{F}$) was then used to compute Green-Lagrange strain ($\mathbf{E} = \frac{\mathbf{1}}{\mathbf{2}}(\mathbf{C} - \mathbf{I})$) in the local coordinate system of each surface element. Principal strains were obtained from the eigenvalues of the in-plane strain tensor **E**, and the maximum principal strain was stored in the mesh nodes as the local strain measure.

2.3.2 Registration

A custom software pipeline developed in Python (version 3.9.22, Python Software Foundation) was used to combine the aortic wall mesh containing the local strain data with the wall shear stress (WSS) point cloud. To enable spatial correspondence between datasets, the geometries were first clipped consistently at the aortic root and centerlines were generated for each mesh using the Vascular Modeling Toolkit package (Izzo et al. 2018). The surfaces were then registered using a two-step approach. First, an initial centerline-based alignment was applied to account for the global coordinate differences, followed by an iterative closest point registration transform using the VTK package (Schroeder et al. 2006) to refine the surface alignment. After registration, WSS values from the point cloud were transferred onto the aortic wall mesh, resulting in a single patient-specific wall mesh containing localized strain and WSS data for subsequent analysis.

Following registration, selection of specimen location was performed using a graphical user interface (GUI) designed for analysis of the in vivo mesh. During surgery, a series of images are captured that allow for identification of surface features of the aneurysm, as well as sketches and approximate dimensions of the regional and specimen divisions. These are used to identify the specimen location on the mesh as accurately as possible. Selection of a specimen location in the GUI contains the mesh nodes within a 6mm radius sphere for visualization, and the data contained within the sphere is averaged to produce a single value of WSS and strain associated with that specimen location.

Additional non-invasive, patient-specific parameters considered for the analysis were patient age and aneurysm diameter.

2.4 Statistical analysis

Continuous variables were assessed for normality using the Shapiro-Wilk test and associations between variables were evaluated using Pearson's correlation (for normal data) or Spearman's rank correlation (for non-normal data). To compare groups, the Kruskal-Wallis *H* test (for non-normal data) or ANOVA test (for normal data) was employed. All statistical analysis was completed using the SciPy Stats package (Virtanen et al. 2020). Statistical significance was set at $p<0.05$.

3 RESULTS

3.1 Patient population and specimen overview

Ten BAV patients with AsAA were included in this study for mechanical analysis, with patient demographics presented in Table 1. From these patients, 101 specimens were retrieved and tested mechanically. Specimens were tested as composite tissue (n=53), layer-separated media (n=41), and layer-separated adventitia (n=46). In the case that a specimen ripped prior to completion of the test, the specimen was excluded from the analysis. This occurred in 6 medial specimens and 1 adventitial specimen. A total of 140 biaxial tensile tests, 98 delamination tests, and 245 uniaxial tensile tests were successfully completed.

Table 1. Patient demographics. Age and aortic diameter are presented as mean ± standard deviation.

Characteristic	**Total (n=10)**
Hypertension, %	40
Smoking, %	40
Diabetes, %	0
Sex, male/female, n	9/1
Age, years	56.6 ± 9.8
Aortic diameter, cm	5.1 ± 0.3

3.2 Regional variation of in vivo hemodynamics and deformation

Both wall shear stress (WSS) and in vivo strain varied significantly across anatomical regions. WSS was highest in the greater curvature and anterior regions, whereas strain was highest in the anterior region and lowest in the greater curvature. Among the patient-level characteristics assessed (aneurysm size and patient age), the only significant association was observed between WSS and aneurysm size, with WSS decreasing as aneurysm size increased. Neither WSS nor strain appeared to be significantly associated with age.

Table 2. Regional variation in wall shear stress and in vivo strain.

Region	**n**	**Wall Shear Stress (Pa)**	**Maximum Principal Strain (%)**
Anterior	46	0.90 ± 0.36	8.36 ± 3.8
Greater Curvature	32	1.04 ± 0.38	2.22 ± 1.48
Lesser Curvature	8	0.62 ± 0.24	4.92 ± 2.01
Posterior	13	0.46 ± 0.25	5.48 ± 1.94

3.3 Layer-separated and composite wall mechanics

A summary of the layer-specific and composite wall mechanics is presented in Table 3. When comparing the layers, medial properties tended to be greater at lower levels of deformation, while adventitial properties were greater at higher levels of deformation. In general, the properties of the composite tissue measured between those of the media and adventitia.

Table 3. Mechanical properties of the media, adventitia, and composite tissue.

	Media-Interface	**Interface-Adventitia**	**Composite**
Thickness	0.92 ± 0.18 mm	0.72 ± 0.14 mm	1.67 ± 0.43
Circumferential Direction Mechanics			
Low Tangential Modulus (LTM)	351 ± 140 kPa	239 ± 82.9 kPa	391 ± 144 kPa

High Tangential Modulus (HTM)	978 ± 837 kPa	3102 ± 3449 kPa	1257 ± 866 kPa
Transition Zone Onset (TZo)	Stress: 35.5 ± 16.1 kPa Stretch: 1.10 ± 0.04	Stress: 27.8 ± 14.0 kPa Stretch: 1.12 ± 0.04	Stress: 35.9 ± 15.6 kPa Stretch: 1.10 ± 0.03
Transition Zone End (TZe)	Stress: 81.9 ± 29.9 kPa Stretch: 1.19 ± 0.05	Stress: 137 ± 55.2 kPa Stretch: 1.28 ± 0.04	Stress: 94.1 ± 32.2 kPa Stretch: 1.20 ± 0.07
Energy Loss (EL)	19.7 ± 3.82 %	21.4 ± 4.53 %	20.7 ± 3.53 %
Ultimate Tensile Strength (UTS)	2.17 ± 0.83 MPa	2.32 ± 1.02 MPa	1.95 ± 0.82 MPa
Axial Direction Mechanics			
Low Tangential Modulus (LTM)	294 ± 129 kPa	249 ± 79.6 kPa	327 ± 102 kPa
High Tangential Modulus (HTM)	1156 ± 1373 kPa	3372 ± 3718 kPa	1262 ± 841 kPa
Transition Zone Onset (TZo)	Stress: 30.0 ± 12.9 kPa Stretch: 1.10 ± 0.03	Stress: 30.9 ± 12.4 kPa Stretch: 1.12 ± 0.03	Stress: 31.5 ± 12.5 kPa Stretch: 1.10 ± 0.03
Transition Zone End (TZe)	Stress: 73.7 ± 33.6 kPa Stretch: 1.19 ± 0.05	Stress: 146 ± 61.0 kPa Stretch: 1.28 ± 0.05	Stress: 84.7 ± 30.7 kPa Stretch: 1.20 ± 0.06
Energy Loss (EL)	18.9 ± 4.17 %	20.8 ± 4.48 %	20.0 ± 3.31 %
Ultimate Tensile Strength (UTS)	0.63 ± 0.49 MPa	1.56 ± 0.69 MPa	0.98 ± 0.57 MPa

3.4 Aneurysm diameter shows limited associations with tissue mechanics

No significant associations were observed between aneurysm diameter and mechanical properties of the composite tissue. In the media, aneurysm diameter was associated with parameters describing the high-strain region of the biaxial stress-stretch response. Specifically, increasing diameter was significantly correlated with lower circumferential HTM (ρ = -0.46, p = 0.007) and lower circumferential transition zone end stress (ρ = -0.43, p=0.022). Similar negative trends were observed in the axial direction, although the associations did not reach statistical significance.

In the adventitia, increasing aneurysm diameter was associated with an earlier onset of the transition region. The transition-zone onset stretch decreased significantly with diameter in the axial direction ($\rho = -0.37$, p = 0.015), with a similar but nonsignificant trend in the circumferential direction ($\rho = -0.29$, p = 0.058). No other adventitial mechanical properties were significantly associated with aneurysm diameter.

3.5 Age is associated with layer-specific mechanical remodelling and reduced interfacial strength

Both the media and adventitia exhibited unique age-related changes in mechanical behaviour, significant results are summarized in Table 4. In the media, age was associated primarily with changes in the transition region of the biaxial stress-stretch response. Specifically, the transition zone onset and end stretches decreased significantly in both the circumferential and axial directions. Medial energy loss increased significantly with age in both loading directions.

In the adventitia, the effect of age was mainly observed in stiffness parameters. The low tangential modulus (LTM) decreased with age in both axial and circumferential directions, though the

association reached statistical significance only in the circumferential. In contrast, the high tangential modulus (HTM) increased significantly with age in both directions. Adventitial energy loss also increased with age.

Finally, the interfacial strength was observed to significantly decrease with patient age in both loading directions, indicating reduced resistance to layer separation in older tissue

Table 4. Significant associations between age and mechanical properties of the media, adventitia, and interface.

	Property	**Age effect**	**Circumferential,** ρ (p-value)	**Axial,** ρ (p-value)
Media	TZ-onset stretch	Decrease	-0.35 (0.046)	-0.40 (0.019)
	TZ-end stretch	Decrease	-0.48 (0.0098)	-0.46 (0.0084)
	Energy loss	Increase	0.37 (0.026)	0.42 (0.0096)
Adventitia	LTM	Decrease	-0.44 (0.0033)	-0.27 (0.076)
	HTM	Increase	0.56 ($9.8e10^{-5}$)	0.39 (0.010)
	Energy loss	Increase	0.44 (0.0028)	0.38 (0.011)
Interface	Delamination strength	Decrease	-0.51 (0.0013)	-0.36 (0.029)

3.6 WSS is associated with regional tissue mechanics

In the composite tissue, WSS was significantly associated with energy loss in both directions, with higher WSS corresponding to greater axial ($\rho = 0.55$, $p = 0.0036$) and circumferential ($\rho = 0.51$, $p = 0.0083$) energy loss.

In the media, increasing WSS was associated with decreases in circumferential transition zone onset stress ($\rho = -0.37$, $p = 0.039$) and stretch ($\rho = -0.41$, $p = 0.023$), indicating an earlier transition into the nonlinear portion of the stress-stretch curve. Medial energy loss also increased with WSS in both the axial ($\rho = 0.35$, $p = 0.041$) and circumferential ($\rho = 0.32$, $p = 0.060$) directions, though was not significant in the circumferential direction. In addition, medial thickness was inversely associated with WSS ($\rho = -0.39$, $p = 0.012$), suggesting thinning of the medial layer in specimens that were exposed to elevated WSS. UTS in the media also showed an interesting trend, with a positive correlation with WSS in the axial direction, and negative correlation in the circumferential direction, though not statistically significant (Fig. 4).

Consistent with the composite tissue results, energy loss was the only mechanical parameter of the adventitia significantly associated with WSS, with significant positive associations in both the axial ($\rho = 0.52$, $p = 0.00038$) and circumferential ($\rho = 0.45$, $p = 0.0026$) directions. Interfacial strength was not found to have a significant association with the WSS.

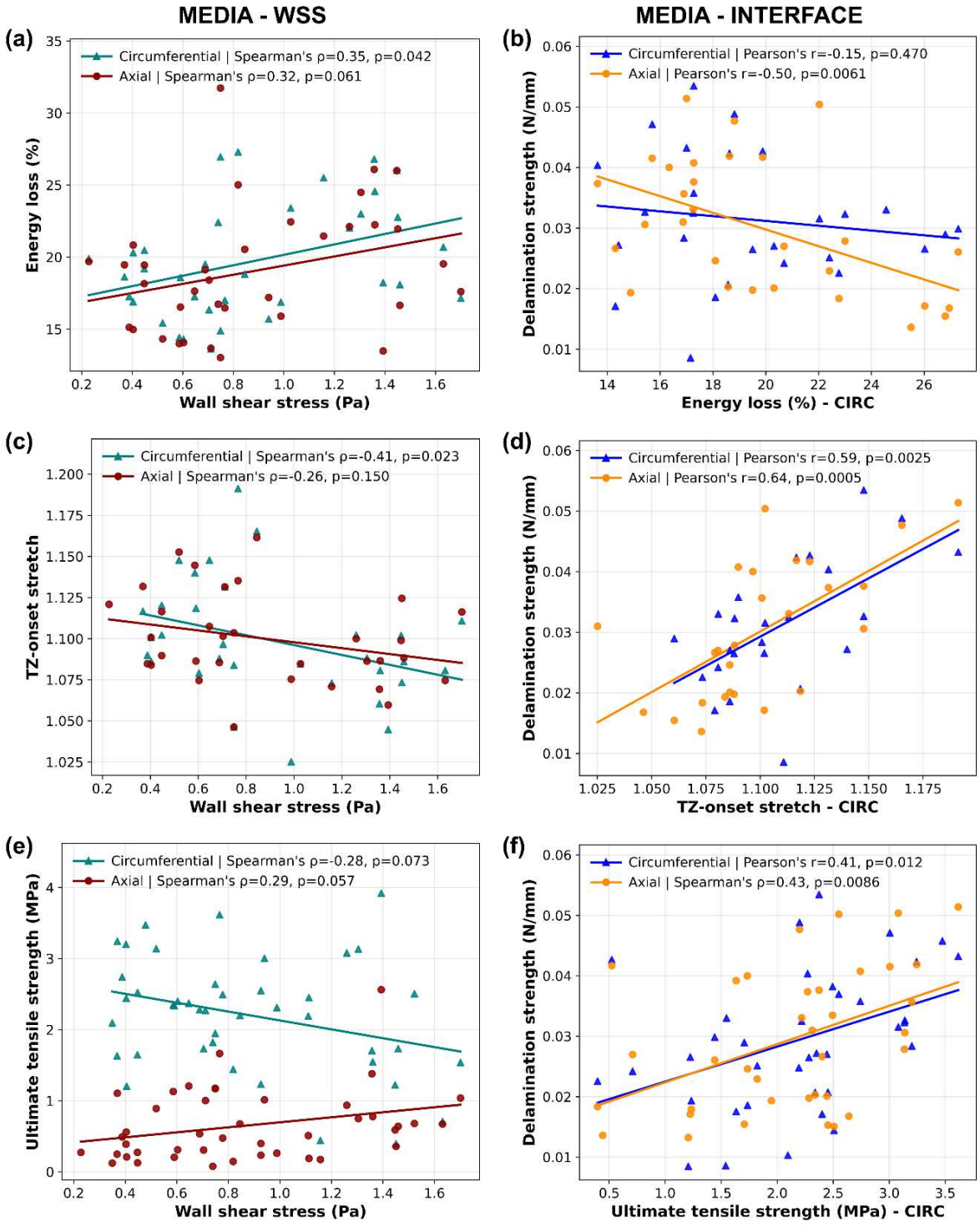

Fig. 4 Associations between WSS, medial mechanics, and interfacial strength. Higher WSS was associated with altered medial mechanics, including (a) increased energy loss, (c) reduced transition-zone onset stretch; and (e) direction-dependent changes in ultimate tensile strength. These same medial properties were also associated with the interfacial delamination strength, as shown in (b), (d), (f).

3.7 In vivo strain relates to tissue strength and stiffness

Most associations between the local maximum principal strain (MPS) and mechanical properties appeared in the axial direction mechanics. In the composite tissue, axial ultimate tensile strength (UTS) was negatively correlated with MPS ($\rho = -0.48$, $p = 0.034$), indicating lower axial failure strength in specimens with higher in vivo strain.

In the media, local MPS was associated with axial stiffness and transition zone parameters. Axial HTM ($\rho = -0.36$, $p = 0.037$) and transition zone onset stress ($\rho = -0.35$, $p = 0.049$) both decreased significantly with increasing MPS, while axial LTM and transition zone end stress showed similar, non-significant trends. Axial UTS in the media also decreased with increasing MPS, although the relationship was not statistically significant.

The adventitia exhibited a similar strain-associated reduction in mechanical properties, particularly in the axial direction. From the uniaxial tensile analysis, MPS was inversely correlated with the axial HTM ($\rho = -0.42$, $p = 0.0068$) and axial UTS ($\rho = -0.40$, $p = 0.0097$), while no significant associations were observed in the circumferential direction. This was also observed in the biaxial results, where axial HTM was found to decrease significantly with increasing MPS.

3.8 Interfacial strength is associated with layer-specific mechanics

To understand variation of interfacial properties in relation to layer-specific properties and aortic wall remodeling, relationships between properties of the layers and the delamination strength of the tissue were evaluated. Delamination strength was associated primarily with the low-strain and transition-zone behaviour of both layers (Table 5).

Strong associations were found between the delamination strength and the transition zone properties of the media, particularly in the circumferential direction (Fig. 4). Greater TZ-onset and TZ-end stretches in both loading directions were positively associated with circumferential and axial delamination strength. The circumferential delamination strength was also found to have a positive correlation with medial UTS in both directions, as well as the medial TZ-end stress. The axial delamination strength was also found to have a negative correlation with circumferential energy loss and positive correlation with medial thickness.

In the adventitia, the interfacial strength was found to relate to the LTM and TZ-onset stress. Greater adventitial LTM and TZ-onset stress were positively associated with delamination strength across both loading and delamination directions.

Table 5. Relationships between delamination strength and properties of the wall layers.

Property		**Delamination Strength Axial**		**Delamination Strength Circumferential**	
		Correlation	p-value	Correlation	p-value
Media - Circumferential	LTM	$\rho = -0.11$	0.57	$\rho = 0.19$	0.35
	TZo Stress	$R = 0.30$	0.13	$R = 0.38$	0.064
	TZo Stretch	**$R = 0.64$**	**<0.001**	**$R = 0.59$**	**0.0025**
	TZe Stress	**$\rho = 0.43$**	**0.047**	**$R = 0.51$**	**0.025**
	TZe Stretch	**$R = 0.67$**	**<0.001**	**$R = 0.64$**	**0.0035**
	EL	**$R = -0.50$**	**0.0061**	$R = -0.15$	0.47
	UTS	**$\rho = 0.43$**	**0.0086**	**$R = 0.41$**	**0.012**
Media - Axial	LTM	$\rho = -0.17$	0.39	$\rho = 0.09$	0.65

	TZo Stress	ρ = 0.15	0.48	ρ = 0.26	0.22
	TZo Stretch	**R = 0.55**	**0.0033**	R = 0.39	0.059
	TZe Stress	ρ = 0.13	0.52	**ρ = 0.43**	**0.049**
	TZe Stretch	**R = 0.63**	**<0.001**	**R = 0.55**	**0.0083**
	EL	ρ = -0.31	0.097	R = -0.03	0.89
	UTS	ρ = 0.24	0.17	**R = 0.45**	**0.0054**
Adventitia - Circumferential	LTM	**ρ = 0.47**	**0.0054**	**R=0.45**	**0.0076**
	TZo Stress	**R = 0.46**	**0.0063**	**R = 0.50**	**0.0029**
	TZo Stretch	R = 0.25	0.15	R = 0.33	0.060
	TZe Stress	**R = 0.35**	**0.044**	R = 0.25	0.15
	TZe Stretch	R = 0.21	0.23	R = 0.16	0.38
	EL	R = -0.29	0.10	R = -0.14	0.44
	UTS	**ρ = 0.35**	**0.036**	R = 0.26	0.12
Adventitia - Axial	LTM	**R = 0.42**	**0.014**	**R = 0.36**	**0.036**
	TZo Stress	**R = 0.41**	**0.017**	R = 0.32	0.062
	TZo Stretch	R = 0.11	0.52	R = 0.10	0.58
	TZe Stress	R = 0.25	0.16	**ρ = 0.40**	**0.020**
	TZe Stretch	ρ = 0.23	0.18	R = 0.24	0.16
	EL	R = -0.21	0.24	R = -0.05	0.79
	UTS	ρ = 0.23	0.18	**ρ = 0.36**	**0.029**

3.9 Relationship between WSS and interfacial strength differs across age groups

Given the significant effect of age on the interfacial strength, the relationship between WSS and delamination strength was subsequently evaluated with the patient cohort divided into age groups: patients ≥ 60 years and patients < 60 years. The age threshold was chosen based on previous studies of elastin-based changes documented between similarly divided BAV age groups (Nightingale et al. 2022b).

In the full cohort, no significant relationship was observed between WSS and delamination strength. When patients were stratified by age, however, higher WSS was significantly negatively correlated with the axial delamination strength in the younger (<60 years) patient group (Fig. 5). In contrast, no significant association was observed in the older group, in which delamination strength was generally lower across the sampled regions as established in 3.8.

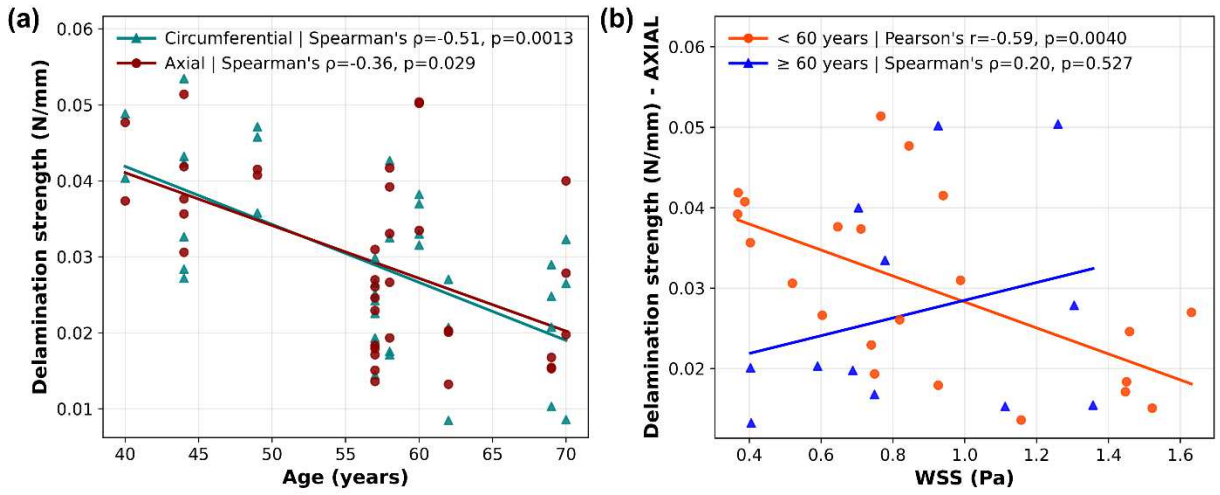

Fig. 5 Relationships between interfacial strength, age, and WSS. (a) Delamination strength decreased with increasing patient age; (b) Following age stratification, higher WSS was associated with reduced axial delamination strength in patients <60 years, whereas no significant association was observed in older patients.

3.10 Collagen gene expression associated with WSS, age, and medial mechanics

RT-qPCR analysis was completed for 39 tissue samples with corresponding in vivo measurements. *COL1A1* and *COL3A1* expression were both significantly and positively correlated with local WSS, while significant negative correlations were observed with patient age. *COL1A1* expression was also found to have an inverse correlation with the aneurysm diameter; however, this relationship was not observed for *COL3A1*. Neither of the genes was found to be associated with MPS. Results are summarized in Table 6.

Table 6. Collagen gene expression and in vivo measures.

In vivo variable	Gene	N	Correlation (Spearman's)	p-value
WSS	*COL1A1*	38	**0.40**	**0.013**
	COL3A1	38	**0.42**	**0.008**
MPS	*COL1A1*	33	0.25	0.15
	COL3A1	33	0.14	0.43
Age	*COL1A1*	39	**-0.43**	**0.006**
	COL3A1	39	**-0.40**	**0.013**
Aneurysm Diameter	*COL1A1*	39	**-0.37**	**0.019**
	COL3A1	39	-0.26	0.12

When assessed for trends with neighbouring, mechanically tested samples, *COL1A1* and *COL3A1* expression were associated with increased medial axial stiffness for both LTM and HTM. *COL3A1* expression was also negatively correlated with medial thickness, with higher expression observed in thinner samples (Table 7). No significant relationships were observed between adventitial mechanical properties and collagen gene expression.

Table 7. Collagen gene expression and mechanical properties of the media.

Biaxial property (media)	Gene	n	Correlation (Spearman's)	p-value
Circumferential LTM	*COL1A1*	10	0.31	0.38
	COL3A1	10	0.50	0.14
Axial LTM	*COL1A1*	10	**0.78**	**0.008**
	COL3A1	10	**0.65**	**0.043**
Circumferential HTM	*COL1A1*	9	0.60	0.09
	COL3A1	9	0.53	0.14
Axial HTM	*COL1A1*	9	**0.73**	**0.025**
	COL3A1	9	**0.73**	**0.025**
Thickness	*COL1A1*	12	-0.39	0.21
	COL3A1	12	**-0.61**	**0.035**

Table 8. Summary of tissue heterogeneity and remodeling characteristics with in vivo parameters.

	↑ **WSS**	↑ **MPS**	↑ **Age**	↑ **Diameter**
Composite	↑ energy loss	↓ UTS ↓ TZ-onset stress[a]		
Media	↑ energy loss ↓ TZ-onset stress ↓ TZ-onset stretch ↓ thickness	↓ UTS[a] ↓ LTM[a] ↓ HTM ↓ TZ-onset stress	↑ energy loss ↓ TZ-onset stretch ↓ TZ-end stretch	↓ HTM ↓ TZ-end stress
Adventitia	↑ energy loss	↓ UTS ↓ HTM	↑ energy loss ↓ LTM ↑ HTM ↓ TZ-onset stress ↓ TZ-end stretch ↓ thickness	↓ TZ-onset stretch
Interface	↓ delamination strength (patients <60 years)		↓ delamination strength	
Gene expression	↑ *COL1A1* ↑ *COL3A1*		↓ *COL1A1* ↓ *COL3A1*	↓ *COL1A1*

[a]non-significant trend (0.05>p>0.10)

4 DISCUSSION

Currently, recommendations for the management of BAV-associated aortic pathology are based on the maximum diameter of the aneurysm, however, continuing revision of these guidelines highlight the uncertainty of best management strategies for this population (Van Ooij et al. 2015; Borger et al. 2018). The objective of this study was to determine whether non-invasive, patient- and imaging-derived variables could provide insight into the local mechanical state of BAV-AsAA tissue. The results suggest that aneurysm diameter alone does not capture the mechanical heterogeneity of the aneurysmal wall. Instead, patient age, local wall shear stress, and local maximum principal strain were each found to be associated with distinct mechanical

characteristics of the aortic wall and layer-specific remodelling, supporting their potential value as markers for future patient-specific risk prediction.

4.1 Diameter provides limited information on wall integrity

Despite its central role in clinical risk assessment, aneurysm diameter was not significantly associated with composite tissue mechanics in this study, although several layer-specific relationships were observed. In the media, diameter was primarily associated high-strain circumferential properties, including the transition-zone end stress and HTM. This relationship is consistent with the expected effects of progressive circumferential expansion, which may promote earlier collagen fibre straightening and recruitment during mechanical loading. This interpretation is further supported by the adventitial results, where increasing diameter was associated with reduced transition-zone onset stretch, again suggesting earlier collagen engagement. However, compared with image-derived WSS, local strain, and patient age, diameter appeared less sensitive to heterogenous characteristics of wall remodelling and mechanical vulnerability, reflecting its role as a global geometric measure rather than a direct indicator of the local tissue integrity.

4.2 Age-related degeneration contributes to wall layer and interfacial mechanics

Age is an easily accessible, non-invasive metric that has been documented to have significant relationships with aortic wall mechanics and microstructure. Increasing age has been associated with structural and biomechanical remodelling of the aortic wall, including elastin fragmentation (Tsamis et al. 2013; Mammoto et al. 2022), collagen accumulation and cross-linking (Tsamis et al. 2013), increased stiffness (HTM) (Kohn et al. 2015; Chung et al. 2020), reduced strength (Ferrara et al. 2016), decreased LTM (Nightingale et al. 2022a), and increased energy loss (Chung et al. 2014). Age-related elastin fragmentation is particularly important in the ascending aorta, where elastin normally provides low-strain elasticity and enables reversible deformation during cyclic loading. Disruption of this elastin network can reduce elastic recoil, alter load transfer to collagen, and contribute to increased stiffness and dissipative mechanical behaviour.

In the present study, age-related changes were found to be heterogeneous by layer. Adventitial mechanics appeared more strongly influenced by age-related stiffness alterations, as reflected by the reduced LTM and increased HTM, whereas medial stiffness did not appear to be age-dependent. Conversely, medial UTS decreased with increasing age, while adventitial UTS was unaffected. Energy loss was the only parameter that increased consistently in both layers, suggesting that aging may broadly impair elastic recovery across the wall, potentially reflecting cumulative elastin loss and extracellular matrix disorganization.

The most significant age-related finding was the relationship between increasing age and reduced delamination strength. This agrees with previous findings that suggest aging is a significant factor in weakening of the aortic wall interface (Angouras et al. 2019a; Horný et al. 2022; Tong et al. 2023; Shahbad et al. 2024). Because delamination strength reflects the resistance of the wall layers to separation, this relationship may have direct relevance to dissection susceptibility. This is especially important in BAV-associated aortic pathologies, as patients often present with aneurysm at significantly younger ages than the general TAV population. Together, these findings indicate that age is an important determinant of baseline wall and interface condition and should be considered when assessing potential wall vulnerability and mechanical degeneration, including interpretation of regional imaging-derived biomarkers such as WSS and strain.

4.3 WSS identifies local medial remodelling and age-dependent interfacial vulnerability

Hemodynamic metrics, particularly wall shear stress (WSS), are of considerable interest in the BAV population as bicuspid valve morphology has been shown to generate eccentric flow patterns and elevated, spatially abnormal WSS compared with age-matched healthy controls (Van Ooij et al. 2015). These altered hemodynamic environments have been implicated in regional aortic wall remodelling, with histopathological studies linking elevated WSS to elastin fragmentation (Bollache et al. 2018), increased local expression of matrix metalloproteinases (Guzzardi et al. 2015; Pasta et al. 2020), and localized wall thinning (Salmasi et al. 2021).

In the present study, image-derived WSS was associated with localized differences in layer-specific biomechanics, with the strongest relationships observed in the media. Specimens exposed to higher WSS demonstrated significantly lower medial transition-zone onset stretch and stress, as well as greater medial energy loss. Energy loss has previously been proposed as a biomechanical marker of AsAA disease progression and has been associated with reduced elastin content and an increased collagen-to-elastin ratio (Chung et al. 2014). Similarly, the transition zone of the stress-stretch response is closely related to the relative contributions of elastin and collagen within the tissue (Nightingale et al. 2022a). A lower transition-zone onset may therefore indicate an earlier shift into the nonlinear, collagen-dominated region of the stress-stretch curve, a behaviour that may reflect elastin degradation, fibrotic or disorganized collagen deposition, or a combination of both. Consistent with this interpretation, elevated WSS was also associated with thinner medial samples and increased expression of *COL1A1* and *COL3A1*, suggesting the presence of collagen-associated remodelling in regions exposed to altered hemodynamic loading. Given that these gene expression changes were associated with medial mechanics, not adventitial, it is likely that this remodelling response is primarily concentrated in the media.

Although the present study did not directly reproduce previous findings linking local WSS with aortic wall stiffening (Nightingale et al. 2024) or delamination strength (Salmasi et al. 2021) in the full cohort, age-stratified analysis suggested that WSS relationships may depend on patient age. When patients were separated into younger (<60 years) and older (≥ 60 years) groups, higher WSS was significantly associated with reduced axial delamination strength in the younger cohort. This finding may indicate that, in younger patients, elevated WSS is associated with localized interfacial weakening, whereas in older patients, interfacial strength may already be reduced more broadly across regions, potentially obscuring local WSS-dependent effects.

WSS and age were also associated with similar changes in several other mechanical characteristics, including increased energy loss and shifting of the transition zone onset and end stretches. Despite these mechanical similarities, the RT-qPCR results suggest that the underlying remodelling processes may differ. Whereas higher WSS was associated with increased *COL1A1* and *COL3A1* expression, increasing age was found to correlate with reduced expression of both collagen genes. This divergence suggests that WSS- and age-associated remodelling may produce overlapping mechanical characteristics through distinct biological mechanisms. Specifically, WSS may reflect an active, localized remodelling response characterized primarily by medial elastin fragmentation and collagen matrix turnover, whereas aging may reflect cumulative matrix degeneration, loss of elastin, and reduced synthetic activity across the aortic wall. As such, MR-derived WSS may strengthen BAV-AsAA risk assessment by providing non-invasive, region-specific insight into

hemodynamically driven wall degeneration and potential early mechanical vulnerability, although age should be considered when interpreting these relationships.

4.4 In vivo strain relates to local stiffness and strength

In vivo strain has been proposed as a non-invasive indicator of regional tissue mechanics, with prior studies demonstrating the feasibility of spatially resolved in vivo aortic strain mapping and regional image-derived mechanical assessment (Wilson et al. 2019). Although it is proposed that heterogenous strain distributions reflect local material properties, few studies have directly compared in vivo strain with spatially matched tissue biomechanics. By combining imaging-based strain analysis with ex vivo mechanical testing, this study provides an integrated assessment of regional deformation and tissue mechanics. The observed relationships between strain and layer-specific stiffness and failure properties suggest that local deformation may provide non-invasive insight into the heterogenous mechanical characteristics of the aneurysmal wall.

Previous in vivo work has shown that thoracic aortic aneurysms may exhibit reduced strain compared with healthy aortas, consistent with reduced deformability or global stiffening of the wall (Wang et al. 2022). When linked to biomechanics, increased strain has been associated with increased failure strength across a mixed patient pool including both healthy and aneurysmal tissue (Dong et al. 2024). However, the relationships assessed in this study were identified within the BAV-AsAA patient cohort, meaning that regions of higher strain were assessed relative to other aneurysmal samples rather than relative to healthy tissue. This distinction is important, as the interpretation of strain seems to differ when evaluating relative mechanical vulnerability within the diseased population. In this study, higher strain was associated with reduced stiffness and failure strength, suggesting that elevated local strain within BAV-AsAA may identify focal regions of reduced biomechanical performance despite the broader expectation of reduced strain in aneurysmal tissue compared with healthy aortas. This result is consistent with the findings of Chiu et al., who evaluated strain from ex vivo testing of AsAA tissue and reported that an increased relative strain was associated with weaker or less mechanically adapted tissue among diseased samples (Chiu et al. 2021). Thus, while reduced strain may reflect tissue stiffening at the global disease level in AsAA patients, locally elevated strain in aneurysmal tissue may indicate regional degeneration or an ineffective remodelling response due to insufficient adaptive remodelling or maladaptive matrix reorganization.

This interpretation is further supported by the directional nature of the mechanical associations observed. Strain was primarily associated with the axial direction mechanics, possibly indicating anisotropic tissue remodeling. Since the 2D optical flow derived strain used in this study primarily captures circumferential deformation, elevated local strain may correspond to regions with altered circumferential load-bearing or increased compliance. These mechanical changes may occur alongside preferential collagen recruitment or matrix reorganization to support circumferential loading, with a corresponding loss of mechanical integrity axially. In this context, reduced axial stiffness (HTM) and failure strength (UTS) may reflect impaired resistance to multiaxial loading, making these regions more susceptible to local failure. The consistency of these relationships across the media and adventitia, in contrast to the more layer-specific WSS findings, further suggest that local strain may capture coordinated through-wall extracellular matrix degeneration or remodelling. As the associations seem to be most evident in mechanical parameters related to

the tissue failure, in vivo strain may be useful for identifying regions of structural degeneration in the aneurysm before gross mechanical failure is evident.

4.5 Limitations and future work

There are several limitations of this work. First, the image-derived in vivo measures each have an associated uncertainty; both WSS and strain analyses are sensitive to image resolution, segmentation, and post-processing assumptions. In particular, the low spatial resolution of the image data in this study may limit the precision of local wall strain measurements. To reduce the influence of absolute value uncertainty, future work may consider analysis using relative or categorical comparisons rather than relying on continuous values. Second, the physical mechanical samples were manually registered to the corresponding "virtual" aorta analysis. As a result, the selected virtual locations may not have perfectly matched the true anatomical locations of the tested specimens, introducing further uncertainty into the local in vivo variables used for mechanical comparisons. Finally, this exploratory study included only 10 BAV-AsAA patients, limiting the generalizability and statistical robustness of the findings. The small cohort reduces confidence in null findings, while the number of comparisons increases the possibility that some observed associations may have occurred by chance. Although multiple tissue samples were analyzed per patient, these are not independent and represent repeated observations within individuals, which should be accounted for in future studies with larger patient cohorts. This study also did not include healthy or TAV-associated aneurysm groups for comparison.

For increased clinical relevance, future work should extend these methods to larger patient cohorts and include TAV-AsAA to determine whether the observed relationships are specific to BAV-associated pathology or reflect broader mechanisms of aneurysm remodelling. Given the cohort size, within-patient sampling, and imaging-resolution and registration limitations, the present findings should be considered hypothesis-generating and require validation in larger, independent cohorts before broader mechanistic conclusions can be drawn.

5 CONCLUSION

Although image-based biomarkers are increasingly being investigated in the context of aneurysm risk assessment, most have focused on relating in vivo metrics to the mechanical behaviour of the composite wall. This study builds on prior evidence of non-uniform remodeling through the aortic wall thickness and presents a novel integration of in vivo imaging-derived metrics with layer-specific mechanical properties. The associations observed within the media and adventitia suggest that mechanically relevant changes may be obscured when only the composite tissue is evaluated. Accounting for this through-thickness heterogeneity is particularly important because the media and adventitia have unique contributions to the mechanical behaviour of the aortic wall and to the failure mechanisms implicated in dissection and rupture.

Our findings indicate that non-invasive, imaging-derived metrics are associated with distinct aspects of layer- and region-specific aortic wall mechanics. While diameter remains the primary clinical metric for risk assessment, it provides limited insight into local tissue properties. Age appears to reflect the baseline mechanical condition of the wall, particularly when considering elastin-dependent mechanical properties such as delamination strength and energy loss. In contrast, the image-derived hemodynamic and deformation measures were associated with layer- and region-specific mechanical behaviour. Higher WSS was associated with medial mechanical properties and potential markers of medial remodelling, while increased local strain was associated

with areas of reduced stiffness and failure strength. These findings support the hypothesis that in vivo WSS and wall strain may provide complementary information regarding regional aortic wall properties. However, their potential clinical relevance and relationship to aneurysm progression or adverse outcomes requires further evaluation in larger patient cohorts with longitudinal follow-up.

References

Angouras DC, Kritharis EP, Sokolis DP (2019a) Regional distribution of delamination strength in ascending thoracic aortic aneurysms. J Mech Behav Biomed Mater 98:58–70. https://doi.org/10.1016/j.jmbbm.2019.06.001

Angouras DC, Kritharis EP, Sokolis DP (2019b) Regional distribution of delamination strength in ascending thoracic aortic aneurysms. J Mech Behav Biomed Mater 98:58–70. https://doi.org/10.1016/j.jmbbm.2019.06.001

Ballasy NN, Jadli AS, Edalat P, et al (2021) Potential role of epicardial adipose tissue in coronary artery endothelial cell dysfunction in type 2 diabetes. FASEB J 35:e21878. https://doi.org/10.1096/fj.202100684RR

Bollache E, Guzzardi DG, Sattari S, et al (2018) Aortic valve-mediated wall shear stress is heterogeneous and predicts regional aortic elastic fiber thinning in bicuspid aortic valve-associated aortopathy. J Thorac Cardiovasc Surg 156:2112-2120.e2. https://doi.org/10.1016/j.jtcvs.2018.05.095

Borger MA, Fedak PWM, Stephens EH, et al (2018) The American Association for Thoracic Surgery consensus guidelines on bicuspid aortic valve–related aortopathy: Full online-only version. J Thorac Cardiovasc Surg 156:e41–e74. https://doi.org/10.1016/j.jtcvs.2018.02.115

Chiu P, Lee H-P, Dalal AR, et al (2021) Relative strain is a novel predictor of aneurysmal degeneration of the thoracic aorta: An ex vivo mechanical study. JVS-Vasc Sci 2:235–246. https://doi.org/10.1016/j.jvssci.2021.08.003

Choudhury N, Bouchot O, Rouleau L, et al (2009) Local mechanical and structural properties of healthy and diseased human ascending aorta tissue. Cardiovasc Pathol 18:83–91. https://doi.org/10.1016/j.carpath.2008.01.001

Chung J, Lachapelle K, Wener E, et al (2014) Energy loss, a novel biomechanical parameter, correlates with aortic aneurysm size and histopathologic findings. J Thorac Cardiovasc Surg 148:1082–1089. https://doi.org/10.1016/j.jtcvs.2014.06.021

Chung JC -Y., Wong E, Tang M, et al (2020) Biomechanics of Aortic Dissection: A Comparison of Aortas Associated With Bicuspid and Tricuspid Aortic Valves. J Am Heart Assoc 9:e016715. https://doi.org/10.1161/JAHA.120.016715

Deveja RP, Iliopoulos DC, Kritharis EP, et al (2018) Effect of Aneurysm and Bicuspid Aortic Valve on Layer-Specific Ascending Aorta Mechanics. Ann Thorac Surg 106:1692–1701. https://doi.org/10.1016/j.athoracsur.2018.05.071

Dong H, Haraldsson H, Leach J, et al (2024) In Vivo Quantification of Ascending Thoracic Aortic Aneurysm Wall Stretch Using MRI: Relationship to Repair Threshold Diameter and Ex Vivo Wall Failure Behavior. J Biomech Eng 146:121009. https://doi.org/10.1115/1.4066430

Fedak PWM, Verma S, David TE, et al (2002) Clinical and Pathophysiological Implications of a Bicuspid Aortic Valve. Circulation 106:900–904. https://doi.org/10.1161/01.CIR.0000027905.26586.E8

Ferrara A, Morganti S, Totaro P, et al (2016) Human dilated ascending aorta: Mechanical characterization via uniaxial tensile tests. J Mech Behav Biomed Mater 53:257–271. https://doi.org/10.1016/j.jmbbm.2015.08.021

Forneris A, Marotti FB, Satriano A, et al (2020) A novel combined fluid dynamic and strain analysis approach identified abdominal aortic aneurysm rupture. J Vasc Surg Cases Innov Tech 6:172–176. https://doi.org/10.1016/j.jvscit.2020.01.014

Guzzardi DG, Barker AJ, Van Ooij P, et al (2015) Valve-Related Hemodynamics Mediate Human Bicuspid Aortopathy. J Am Coll Cardiol 66:892–900. https://doi.org/10.1016/j.jacc.2015.06.1310

Guzzardi DG, Verma S, Fedak PWM (2017) Bicuspid aortic valve aortopathy: mechanistic and clinical insights from recent studies. Curr Opin Cardiol 32:111–116. https://doi.org/10.1097/HCO.0000000000000359

Horný L, Roubalová L, Kronek J, et al (2022) Correlation between age, location, orientation, loading velocity and delamination strength in the human aorta. J Mech Behav Biomed Mater 133:105340. https://doi.org/10.1016/j.jmbbm.2022.105340

Iliopoulos DC, Kritharis EP, Giagini AT, et al (2009) Ascending thoracic aortic aneurysms are associated with compositional remodeling and vessel stiffening but not weakening in age-matched subjects. J Thorac Cardiovasc Surg 137:101–109. https://doi.org/10.1016/j.jtcvs.2008.07.023

Izzo R, Steinman D, Manini S, Antiga L (2018) The Vascular Modeling Toolkit: A Python Library for the Analysis of Tubular Structures in Medical Images. J Open Source Softw 3:745. https://doi.org/10.21105/joss.00745

Kohn JC, Lampi MC, Reinhart-King CA (2015) Age-related vascular stiffening: causes and consequences. Front Genet 06: https://doi.org/10.3389/fgene.2015.00112

Mammoto A, Matus K, Mammoto T (2022) Extracellular Matrix in Aging Aorta. Front Cell Dev Biol 10:822561. https://doi.org/10.3389/fcell.2022.822561

Nightingale M, Gregory A, Sigaeva T, et al (2022a) Biomechanics in ascending aortic aneurysms correlate with tissue composition and strength. JTCVS Open 9:1–10. https://doi.org/10.1016/j.xjon.2021.12.001

Nightingale M, Guzzardi DG, Barker AJ, et al (2022b) Elastin integrity in bicuspid valve-associated aortopathy is associated with altered biomechanical properties and influenced by age. Ann Cardiothorac Surg 11:426–435. https://doi.org/10.21037/acs-2022-bav-17

Nightingale M, Scott MB, Sigaeva T, et al (2024) Magnetic resonance imaging-based hemodynamic wall shear stress alters aortic wall tissue biomechanics in bicuspid aortic valve patients. J Thorac Cardiovasc Surg 168:465-476.e5. https://doi.org/10.1016/j.jtcvs.2022.12.021

Pape LA, Tsai TT, Isselbacher EM, et al (2007) Aortic Diameter ≥5.5 cm Is Not a Good Predictor of Type A Aortic Dissection: Observations From the International Registry of Acute Aortic Dissection (IRAD). Circulation 116:1120–1127. https://doi.org/10.1161/CIRCULATIONAHA.107.702720

Pasta S, Agnese V, Gallo A, et al (2020) Shear Stress and Aortic Strain Associations With Biomarkers of Ascending Thoracic Aortic Aneurysm. Ann Thorac Surg 110:1595–1604. https://doi.org/10.1016/j.athoracsur.2020.03.017

Perez ZG, Zafar MA, Velasco JJ, et al (2023) Aortic Size at the Time of Type A and Type B Dissections. Ann Thorac Surg 116:262–268. https://doi.org/10.1016/j.athoracsur.2023.03.037

Saliba E, Sia Y, Dore A, El Hamamsy I (2015) The ascending aortic aneurysm: When to intervene? IJC Heart Vasc 6:91–100. https://doi.org/10.1016/j.ijcha.2015.01.009

Salmasi MY, Pirola S, Sasidharan S, et al (2021) High Wall Shear Stress can Predict Wall Degradation in Ascending Aortic Aneurysms: An Integrated Biomechanics Study. Front Bioeng Biotechnol 9:750656. https://doi.org/10.3389/fbioe.2021.750656

Schroeder WJ, Martin K, Lorensen WE, et al (2006) The visualization toolkit: an object-oriented approach to 3D graphics ; [visualize data in 3D - medical, engineering or scientific ; build your own applications with C++, Tcl, Java or Python ; includes source code for VTK (supports UNIX, Windows and Mac)], 4. ed. Kitware, Inc, Clifton Park, NY

Shahbad R, Kamenskiy A, Razian SA, et al (2024) Effects of age, elastin density, and glycosaminoglycan accumulation on the delamination strength of human thoracic and abdominal aortas. Acta Biomater 189:413–426. https://doi.org/10.1016/j.actbio.2024.10.010

Sokolis DP, Kritharis EP, Iliopoulos DC (2012) Effect of layer heterogeneity on the biomechanical properties of ascending thoracic aortic aneurysms. Med Biol Eng Comput 50:1227–1237. https://doi.org/10.1007/s11517-012-0949-x

Tong J, Xin Y-F, Zhang Z, et al (2023) Effect of hypertension on the delamination and tensile strength of ascending thoracic aortic aneurysm with a focus on right lateral region. J Biomech 154:111615. https://doi.org/10.1016/j.jbiomech.2023.111615

Tsamis A, Krawiec JT, Vorp DA (2013) Elastin and collagen fibre microstructure of the human aorta in ageing and disease: a review. J R Soc Interface 10:20121004. https://doi.org/10.1098/rsif.2012.1004

van der Walt S, Schönberger JL, Nunez-Iglesias J, et al (2014) scikit-image: Image processing in Python. https://doi.org/10.48550/ARXIV.1407.6245

Van Ooij P, Potters WV, Collins J, et al (2015) Characterization of Abnormal Wall Shear Stress Using 4D Flow MRI in Human Bicuspid Aortopathy. Ann Biomed Eng 43:1385–1397. https://doi.org/10.1007/s10439-014-1092-7

Virtanen P, Gommers R, Oliphant TE, et al (2020) SciPy 1.0: fundamental algorithms for scientific computing in Python. Nat Methods 17:261–272. https://doi.org/10.1038/s41592-019-0686-2

Wang D, Chayer B, Destrempes F, et al (2022) Deformability of ascending thoracic aorta aneurysms assessed using ultrafast ultrasound and a principal strain estimator: In vitro evaluation and in vivo feasibility. Med Phys 49:1759–1775. https://doi.org/10.1002/mp.15464

Ward C (2000) Clinical significance of the bicuspid aortic valve. Heart 83:81–85. https://doi.org/10.1136/heart.83.1.81

Wilson JS, Taylor WR, Oshinski J (2019) Assessment of the regional distribution of normalized circumferential strain in the thoracic and abdominal aorta using DENSE cardiovascular magnetic resonance. J Cardiovasc Magn Reson 21:59. https://doi.org/10.1186/s12968-019-0565-0

Wu J, Zeng W, Li X, et al (2023) Aortic size distribution among normal, hypertension, bicuspid, and Marfan populations. Eur Heart J - Imaging Methods Pract 1:qyad019. https://doi.org/10.1093/ehjimp/qyad019

Yang M, Nie Z, Yue H, et al (2025) Aortopathy associated with bicuspid aortic valve: advances in clinical and hemodynamics research. Front Physiol 16:1576072. https://doi.org/10.3389/fphys.2025.1576072